THE JOURNAL OF PHYSICAL CHEMISTRY B

Article

pubs.acs.org/JPCB

Regulation of the Electric Charge in Phosphatidic Acid Domains

Wenjie Wang, Nathaniel A. Anderson, Alex Travesset, and David Vaknin*

Ames Laboratory and Department of Physics and Astronomy, Iowa State University, Ames, Iowa 50011, United States

Supporting Information

ABSTRACT: Although a minor component of the lipidome, phosphatidic acid (PA) plays a crucial role in nearly all signaling pathways involving cell membranes, in part because of its variable electrical charge in response to environmental conditions. To investigate how charge is regulated in domains of PA, we applied surface-sensitive X-ray reflectivity and fluorescence near-total-reflection techniques to determine the binding of divalent ions (Ca^{2+} at various pH values) to 1,2-dimyristoyl-*sn*-glycero-3-phosphate (DMPA) and to the simpler lipid dihexadecyl phosphate (DHDP) spread as monolayers at the air/water interface. We found that the protonation state of PA is controlled not only by the pK_a and local pH but also by the strong affinity to PA driven by electrostatic correlations from divalent ions and the cooperative effect of the two dissociable protons, which dramatically enhance the surface charge. A precise theoretical model is presented providing a general framework to predict the protonation state of PA. Implications for recent experiments on charge regulation by hydrogen bonding and the role of pH in PA signaling are discussed in detail.

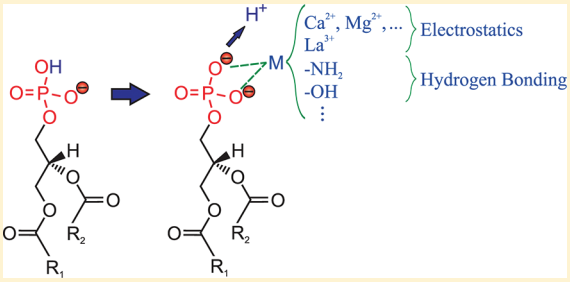

INTRODUCTION

Originally, cellular and organelle lipids were considered to be passive components that provide an impenetrable wall, whereas proteins actively transfer signals across the membranes. It has been gradually recognized, however, that lipids play a fundamentally active role in almost all processes in cellular membranes. For instance, sphingosines, ceramides, and sphingolipids are active as secondary messengers in the regulation of cell growth and apoptosis.[1] Phosphatidic acid (PA) and the phosphoinositides (PIPs), phosphorylated products of phosphatidylinositol, have been found to be crucial to virtually all signaling pathways across cell membrane.[2−4] Even the more common phospholipids such as phosphatidylcholine (PC), phosphatidylethanolamine (PE), and phosphatidylserine (PS) have been implicated in the recruitment of proteins during signaling.[5,6]

The extraordinary functions that PA and other lipids perform lie in their versatile physicochemical interactions with neighboring phospholipids, proteins, and other molecules. Central to this versatility is the ability of PA to regulate its electric charge[7] in response to environmental conditions (e.g., pH, specific ion concentrations). The electric charge of an acid is directly related to its protonation state, which is predicted from the pK_a value and the *local* concentration of protons, $[H^+] = 10^{-pH}$, according to the Henderson−Hasselbalch formula

$$p_d = \frac{1}{1 + 10^{pH_l - pK_a}} \quad (1)$$

where p_d is the probability that the molecule is deprotonated. The subscript of pH_l emphasizes that it is the *local* pH, as opposed to the bulk pH, entering into the Henderson−Hasselbalch formula. For example, if the molecule is within a negatively charged interface, as all real membranes are, the local pH will differ significantly from its bulk value, as the positively charged proton is attracted to the interface whereas the neutral water is not, thus decreasing its local pH value. Within Poisson−Boltzmann theory, this effect is quantified as $10^{-pH_l} = 10^{-pH} \exp[-e\phi(0)]$, where pH is the bulk value and $\phi(0)$ is the contact potential value in units of k_BT/e (k_B and T are Boltzmann constant and temperature, respectively). Equation 1 has been well documented in the literature and rigorously tested in monolayers in contact with monovalent ion solutions.[8,9] Thus, for a molecule with a few pK_a values (one per each degree of protonation), the charge can be readily predicted by generalizing eq 1. NMR studies, however, have revealed a considerably more nuanced picture: The protonation state of PA also depends on its proximity to other lipids or proteins with the ability to form hydrogen bonds with the PA phosphomonoester group. This effect is called the "electrostatic/hydrogen-bond switch mechanism"[10−13] and results in a PA charge that depends not only on the local pH but also on the specific neighborhood of the PA molecule. Yet, in domains of PA without the presence of lipid species or proteins, NMR studies have established that eq 1 should correctly predict the protonation state.[12]

Recent X-ray studies of PA monolayers strongly suggest that, in the presence of divalent[14,15] and trivalent[16] ions, PA is doubly deprotonated (charge 2−) at physiological pH, a result also suggested by numerical simulations.[17] With the measured pK_a values of PA,[10] this double deprotonation is inconsistent

Received: April 20, 2012
Revised: May 18, 2012
Published: May 19, 2012

   dx.doi.org/10.1021/jp303840a | J. Phys. Chem. B 2012, 116, 7213−7220

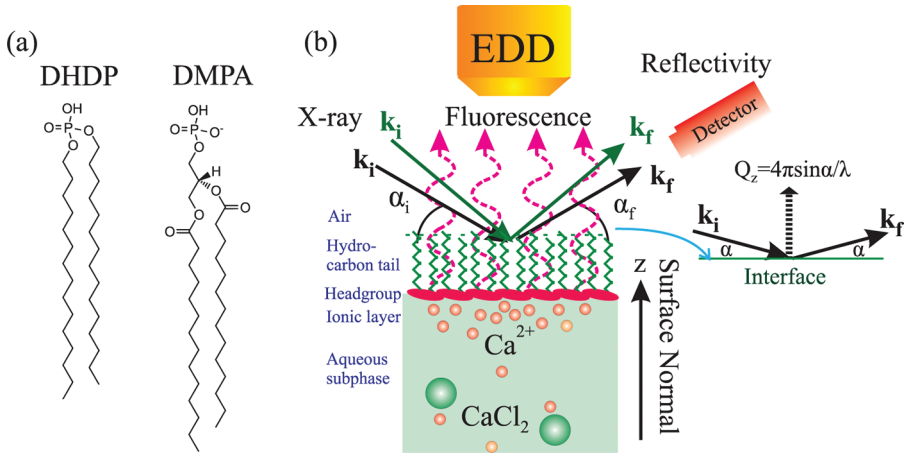

Figure 1. Schematic representations of (a) DHDP and DMPA molecules and (b) the experimental setup for XR and XF measurements.

with the generalized formula for eq 1 as elaborated below, demonstrating that multivalent ions have an additional effect in deprotonating PA and other lipids. In this work, we investigate this effect by considering monolayers of 1,2-dimyristoyl-*sn*-glycero-3-phosphate (DMPA) and comparing its behavior with that of the synthetic lipid dihexadecyl phosphate (DHDP), which is identical to PA except that it has a phosphodiester group (see Figure 1a) and only two protonation states (one and zero protons) compared to the three of PA. In this way, DHDP provides a convenient probe to identify effects related to the second proton in PA. This study focuses on Ca^{2+} ion solutions at a fixed concentration of 1 mM. Although the Ca^{2+} concentration is much smaller in resting cells (below micromolar), it can be temporarily enhanced (in the millimolar range or higher) through transient responses to external cues.[18] Furthermore, physiological concentrations of the related divalent Mg^{2+} ions are in the millimolar range, thus providing additional relevance for this study.

The role played by divalent ions in deprotonating interfaces is a general effect. Silica interfaces provide one of the most studied examples.[19−21] Particularly relevant are the elegant results reported by Labbez et al.,[21] whose detailed Monte Carlo simulations showed evidence that the observed differences in titration curves for monovalent and divalent ions can be explained by electrostatic correlations. The relation of previous work to the case of PA is discussed in the conclusions.

The interactions of Ca^{2+} and phosphate moieties in various phospholipids of biomembranes have been characterized using various techniques, such as differential scanning calorimetry,[22] microelectrophoresis,[23] spectroscopic techniques (infrared, Raman, and NMR),[12,22,24−27] and X-ray scattering.[22,26] These studies mostly focused on the dynamical properties of phosphate−Ca^{2+} bonding and the concomitant conformation changes in a bilayer structure in the presence of Ca^{2+} ions. They showed that Ca^{2+} ions may form complexes with the phosphate moieties, squeeze out the hydration water molecules from the phosphate moieties, and bridge the neighboring phosphate moieties. On the other hand, surface-sensitive X-ray scattering techniques, namely, X-ray specular reflectivity (XR) and grazing-incidence X-ray diffraction, are superior in the characterization of the interfacial structures (scattering length density normal to the surface and in-plane periodic molecular arrangement) of lipid monolayers on aqueous subphases on the molecular length scale. The application of these surface-sensitive X-ray techniques to Ca^{2+}−phospholipid membrane systems has shed more light on the interfacial processes of physical or chemical origin.[15,28−31] In addition, we employed an X-ray spectroscopic technique, namely, X-ray near-total-reflection fluorescence (XF), that enables specific identification and enumeration of ions adsorbed to the monolayer.[32−34]

■ EXPERIMENTAL DETAILS

Ion bulk concentrations were prepared using solutions of calcium chloride ($CaCl_2$), obtained from Sigma-Aldrich. The concentrations of aqueous solutions were kept at 1 mM (10^{-3} M). Ultrapure water (Millipore, Milli-Q, 18.2 MΩ cm) was used for all subphase preparations. Hydrochloric acid (HCl) and potassium hydroxide (KOH) were used to regulate pH levels. The bulk solutions of $CaCl_2$ used in X-ray measurements were prepared at three pH levels, namely, 3.4, 5.8, and 7.8. Langmuir monolayers were prepared by spreading dihexadecyl phosphate (DHDP, $C_{32}H_{67}O_4P$, CAS No. 2197-63-9, purchased from Sigma Chemical Co.) or 1,2-dimyristoyl-*sn*-glycero-3-phosphate (sodium salt) (DMPA, $C_{31}H_{60}O_8PNa$, CAS No. 80724-31-8, purchased from Avanti Lipids, Inc.) onto an aqueous surface. Schematic illustrations of both molecules are shown in Figure 1a. The pure lipid (DHDP or DMPA) was dissolved in 3:1 chloroform/methanol solutions and spread at gas/water interfaces in a thermostatic, solid Teflon Langmuir trough kept at constant temperature (20 °C). Compression of the monolayer by a motorized Teflon bar, at a rate of ∼1 Å^2 per molecule per minute, was started 10−15 min after spreading of the monolayer to allow for evaporation of solvent, and the surface pressure was recorded with a microbalance using a filter-paper Wilhelmy plate.[35] X-ray measurements were conducted at a constant surface pressure Π (∼30 ± 5 mN/m) to ensure a densely packed monolayer, corresponding to a molecular area of A = 41 ± 3 Å^2.[35] To minimize radiation damage due to the formation of radicals and to reduce background scattering from air, the encapsulated trough was continuously purged with water-saturated helium during the X-ray experiments.

X-ray reflectivity (XR) and near-total-external-reflection fluorescence (XF) studies were conducted on a liquid-surface diffractometer at Ames Laboratory using a Rigaku UltraX-18 X-ray source generator with a copper rotating anode (Cu K_α, wavelength λ = 1.54 Å) operating at 50 kV and 250 mA. A monochromatic X-ray beam of wavevector $\mathbf{k}_i$ and wavelength λ (incident wavevector magnitude $|\mathbf{k}_i| = 2\pi/\lambda$) was incident at an angle α_i with respect to the liquid surface and was detected at

dx.doi.org/10.1021/jp303840a | J. Phys. Chem. B 2012, 116, 7213−7220

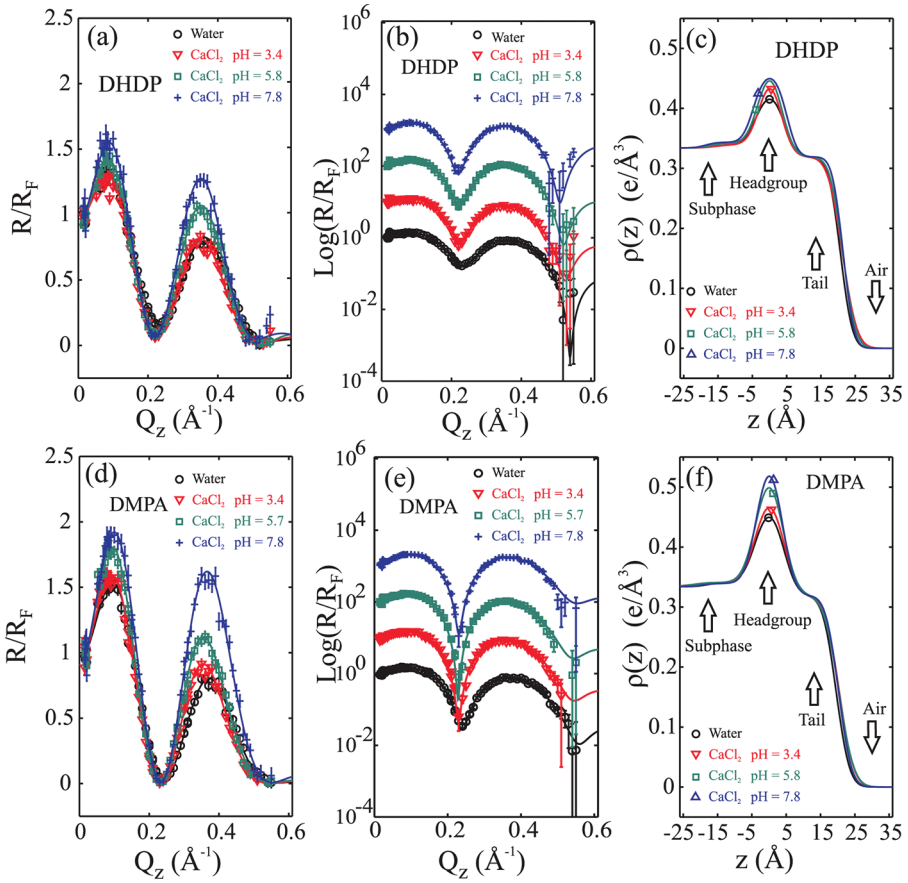

Figure 2. Measured normalized reflectivities (on linear and logarithmic scales) and their corresponding ED profiles for (a–c) DHDP and (d–f) DMPA. The reflectivity curves on semilogarithmic scales are shifted vertically by decades for clarity. The ED profiles in panels c and f were used to calculate the reflectivities (solid lines through R/R_F data). The ED profiles are shifted horizontally for clarity.

an outgoing angle α_f with a final wavevector $\mathbf{k}_f$ and $|\mathbf{k}_f| = |\mathbf{k}_i|$. For specular X-ray reflectivity measurement, $\alpha_i = \alpha_f = \alpha$, as shown in Figure 1b. A Ge(111) crystal was used to select the Cu K_α characteristic radiation (X-ray energy E = 8.05 keV, λ = 1.54 Å) and to steer the downstream beam from the horizon onto the liquid surface at the desired incidence angle α_i. The momentum transfer of X-rays, $\mathbf{Q}$, is defined in terms of the incident and reflected beams as $\mathbf{Q} = \mathbf{k}_f - \mathbf{k}_i$. It is strictly oriented along the surface normal with a z component of $Q_z = 4\pi \sin \alpha/\lambda$, as shown in Figure 1b. Specular X-ray reflectivity (XR), $R(Q_z)$, is measured as a function of Q_z. After background subtraction and scaling, it is normalized to the calculated Fresnel reflectivity R_F from a sharp, flat air–water interface. The parametrized electron density (ED) profile, $\rho(z)$, across an interface with its z axis normal to the aqueous surface can be extracted from refinements of R/R_F data using Parratt's recursive method .[8,9,35−40]

As an X-ray wave travels through a liquid, elements in its path are excited and emit photons at characteristic X-ray energies (X-ray fluorescence). To measure the fluorescence intensity at each value of Q_z, an energy-dispersive detector (EDD) was placed above the liquid surface (~2 cm) with its detector window subtending the illuminated surface, as shown in Figure 1b. Other than Ca K_α (~3.7 keV) and K_β (~4.0 keV) radiation, the unresolved Cl K_α and K_β (~2.6 keV) emission lines and the quasi-elastic scattering of the primary beam (E = 8.05 keV) were also collected by the EDD. Fluorescence signals from K^+ ions (present because of pH regulation by KOH) were below the detection limit of the EDD at all Q_z values. The fluorescence from pure water was measured as background and subtracted from that of samples. To determine the amount of surface-bound Ca^{2+} ions, the fluorescence intensity of Ca^{2+} in the presence of the monolayer was normalized to that of pure $CaCl_2$ with a concentration of 1 mM.[15,32] In general, the analysis of the angular dependence of fluorescence intensity can yield more precise surface densities of absorbed elements and spatial distributions with respect to the surface.[33−35,41−43] The fluorescence from the scattered primary beam and chlorine was monitored and evaluated to ensure the consistency of the performance of the silicon-drift diode EDD. The curve fitting of the X-ray reflectivity and fluorescence data represented by symbols (circles, squares, and so forth) and associated error bars due to counting statistics are based on parametrized models and were obtained through a nonlinear least-squares method. χ^2 is defined as the sum square of differences between model-dependent calculations and experimental data weighted by the uncertainty. The refinement of parameters was carried out through minimization of χ^2 to its minimum value χ_{min}^2.

RESULTS

X-ray Specular Reflectivity. The normalized reflectivities (R/R_F) of monolayers spread on pure water and $CaCl_2$ solutions at various bulk pH levels are shown in Figure 2. The same reflectivity data are displayed in linear scale and logarithmic scale separately to accentuate different features. The oscillatory reflectivity is manifestation of a layered structure on

dx.doi.org/10.1021/jp303840a | J. Phys. Chem. B 2012, 116, 7213−7220

Table 1. Numbers of Surface-Bound Calcium Ions per Molecule (DHDP or DMPA) Calculated from the Best Fit of the Q_z Dependence of the Fluorescence Intensity and Reflectivity Data at Three Bulk pH Levels

method	stoichiometric ratio	pH 3.4	pH 5.8	pH 7.8
		DHDP		
fluorescence[a]	Ca^{2+}/DHDP	$0.25^{+0.07}_{-0.06}$	$0.35^{+0.09}_{-0.07}$	$0.49^{+0.12}_{-0.10}$
reflectivity	Ca^{2+}/DHDP	<0.20	0.49 ± 0.29	0.96 ± 0.28
	$[Ca(H_2O)_4)]^{2+}$/DHDP	<0.10	0.27 ± 0.16	0.53 ± 0.15
	$[Ca(H_2O)_6)]^{2+}$/DHDP	<0.08	0.20 ± 0.12	0.40 ± 0.12
		DMPA		
fluorescence[a]	Ca^{2+}/DMPA	$0.35^{+0.10}_{-0.07}$	$0.58^{+0.13}_{-0.11}$	$1.02^{+0.20}_{-0.20}$
reflectivity	Ca^{2+}/DMPA	0.31 ± 0.31	0.88 ± 0.32	1.1 ± 0.33
	$[Ca(H_2O)_4)]^{2+}$/DMPA	0.17 ± 0.17	0.50 ± 0.19	0.62 ± 0.21
	$[Ca(H_2O)_6)]^{2+}$/DMPA	0.13 ± 0.13	0.37 ± 0.14	0.46 ± 0.15

[a]Upper and lower bounds correspond to the 68.3% confidence level.

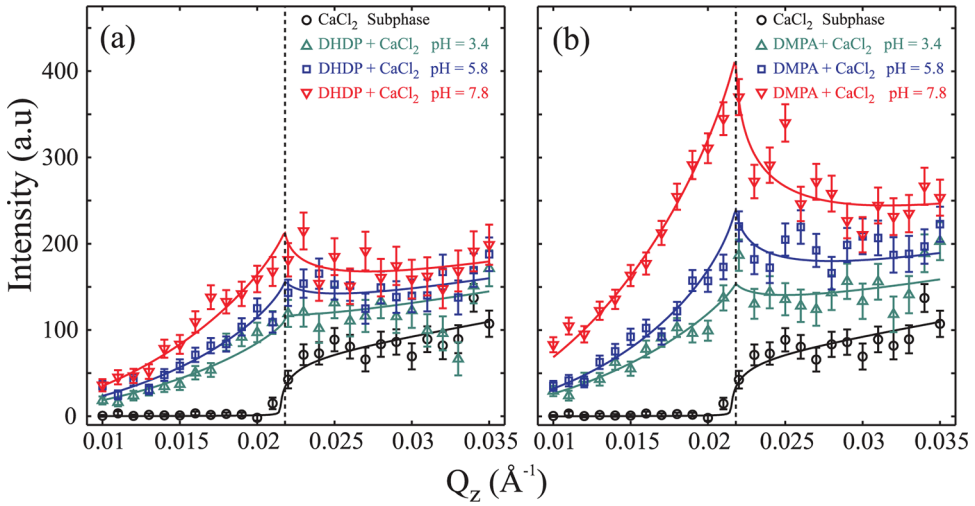

Figure 3. Fluorescence intensities of calcium emission lines (K_α and K_β) as a function of Q_z for (a) DHDP and (b) DMPA spread over 1 mM $CaCl_2$ solutions at various bulk pH levels as indicated. Each data point represents the fluorescence intensity integrated over emitting photon energies from 3.5 to 4.5 keV. Each error bar represents one standard deviation. The vertical dashed lines indicate Q_c (corresponding to the critical angle α_c). Solid lines through the data points are best fit in terms of an analytical model.[35,41]

the aqueous surface. Two qualitative features of reflectivity curves are considered to be related to the molecular arrangements normal to the interfaces.[44] One is the magnitude of the reflectivity, particularly the first maximum at $Q_z \approx 0.1$ Å^{-1}, which is proportional to the surface excess electron density with respect to the subphase and is best seen on the linear scale. The other is the Q_z value corresponding to the first reflectivity minimum (at $Q_z \approx 0.2$ Å^{-1}), which is inversely proportional to film thickness and is best seen on the logarithmic scale. Panels a and d of Figure 2 show that the reflectivities for the DMPA and DHDP monolayers over pure water are smallest over the entire Q_z range investigated. The presence of $CaCl_2$ increases the reflectivity in general, evidence for ion accumulation at the lipid interfaces. Panels b and e of Figure 2 show that the first minima in reflectivity data for $CaCl_2$ solutions are slightly shifted to smaller Q_z compared to those of the corresponding monolayers on water. This is consistent with the binding of ions, but this minute change indicates that the Ca^{2+} binding does not significantly change the film thickness; that is, Ca^{2+} ions are to a large extent laterally intercalate among the lipids' headgroups. Figure 2 also shows that the normalized reflectivities from monolayers over $CaCl_2$ solutions consistently increase with pH over the entire Q_z range, indicating pH-dependent accumulation of Ca^{2+} ions at the interface.[41,42,45]

The surface excess electrons with respect to the subphase can be assigned to each moiety (PA molecules, Ca^{2+} ions, or calcium complexes) on the surface in terms of a space-filling model given the structure and composition, assuming that each moiety is known (for details, see the Supporting Information).[14,35,46] A Ca^{2+} ion can exist in its hydrated state in aqueous media in the form of $[Ca(H_2O)_x]^{2+}$ complex, where x is the number of the coordinated water molecules in the first hydration shell around the central Ca^{2+}.[47−50] Here, three scenarios are examined, namely, $x = 0$ for a pure Ca^{2+} ion forming a complex with PA, $x = 4$ for a partial dehydration of the $[Ca(H_2O)_x]^{2+}$ octahedron bridging two charged moieties on surfaces, and $x = 6$ for a $[Ca(H_2O)_x]^{2+}$ octahedron rising to the surface without losing its hydration shell. The fractions of Ca^{2+} per PA molecules thus obtained are summarized in Table 1.

X-ray Fluorescence. Fluorescence intensities, integrated over the Ca K_α and K_β emitting photon energies (E = 3.5−4.5 keV), are displayed as functions of Q_z in Figure 3. The fluorescence intensity for 1 mM $CaCl_2$ bulk solution is practically zero below Q_c, indicating that the amount of Ca^{2+} probed within the volume determined by the X-ray penetration depth is below the EDD's detection limit. Above Q_c, an abrupt increase in fluorescence intensity occurs because of the dramatic increase of the X-ray penetration depth into the

dx.doi.org/10.1021/jp303840a | J. Phys. Chem. B 2012, 116, 7213−7220

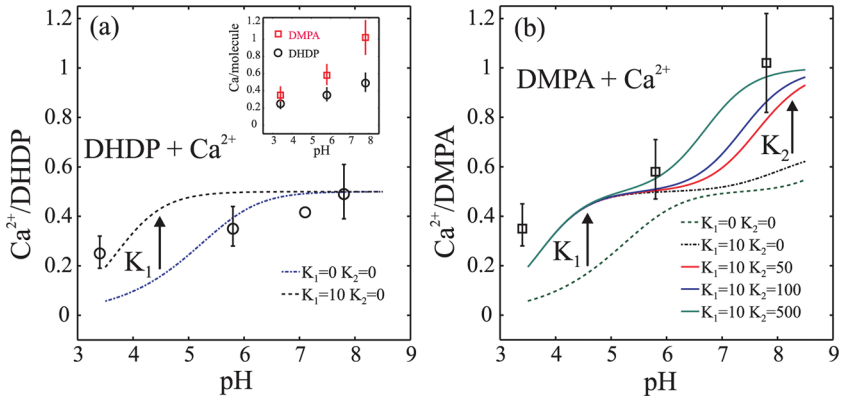

Figure 4. Fractions of Ca^{2+} ions per lipid molecule for (a) DHDP and (b) DMPA based on fluorescence data (circles and squares symbols) and theoretical calculations (lines) as a function of pH. The dotted line corresponding to $K_1 = 0$, $K_2 = 0$ was calculated using eq 2; the other lines were calculated with eq 5. The inset in panel a is a comparison of experimental results from XF.

bulk.[37−39] In general, for $Q_z < Q_c$, the evanescent X-ray wave penetrates into the aqueous medium to within a depth of 50−100 Å, whereas for $Q_z > Q_c$, the penetration depth into the bulk is determined by the beam attenuation due to scattering processes and absorption. In the presence of monolayers, Figure 3 shows that the fluorescence intensity is higher than that of the bare solution over the whole Q_z range and that it peaks at Q_c. This is clear evidence for adsorbed Ca^{2+} ions at the surface. In general, the signal over the whole Q_z range consists of a superposition of contributions from the interfacial ions and from bulk ions. (The genuine fluorescence signal from the interfacial ions can be obtained by subtracting the signal of the bare surface solution from that of the monolayer-covered solution.) Figure 3 shows that the fluorescence intensity in the presence of DHDP and DMPA increases with pH. This is consistent with the XR measurements, which show a similar trend of increasing amounts of surface-bound Ca^{2+} with increasing pH. In addition, Figure 3 shows that the maximum amount of surface-bound Ca^{2+} for the DMPA monolayer at pH 7.8 is almost twice that for the DHDP monolayer at the same pH. Quantitative analysis of the fluorescence data yields the number of Ca^{2+} ions per PA (or DHDP) molecule by calibrating the scale factor of the signal to that of a known concentration of Ca^{2+} bulk solution (for details, see the Supporting Information).[35] These results are summarized in Table 1 and Figure 4.

Table 1 summarizes both XR and XF consistently demonstrating the increase trend of Ca^{2+} per lipid molecule with bulk pH. The XF technique determines the surface-bound ions directly, in particular, showing that, at high pH, the lipid molecules reach their 0 protonation state, that is, ∼0.5 and ∼1.0 Ca^{2+} ion per DHDP and DMPA, respectively. Although XR determines the surface excess electron number accurately, its assignment to the number of Ca^{2+} ions at the interface is model-dependent. Specifically, the determination relies on the choice of the hydration state of the bound Ca^{2+} ions. The free, dehydrated Ca^{2+} ion choice yields the upper bound on the number of calcium ions per lipid molecule, whereas the fully hydrated $[Ca(H_2O)_6]^{2+}$ complex yields the lower bound. In Table 1, we list three models ($([Ca(H_2O)_x]^{2+}$, where $x = 0,4,6$) for comparison with the XF results. We argue that it is less likely for a $[Ca(H_2O)_6]^{2+}$ cluster to bind to a phosphate moiety of DMPA or DHDP directly without (partial) dehydration. For instance, at pH 7.8, bare Ca^{2+} ions and $[Ca(H_2O)_4]^{2+}$ clusters can bind to DMPA and DHDP molecules, respectively.

DISCUSSION

The experimental evidence summarized in Figure 4 shows that, as the bulk pH increases, the average charge of DMPA gradually diverges from that of DHDP. This difference can be readily attributed to the second deprotonation of DMPA, which is impossible for DHDP. Slight generalization of eq 1 to the two pK_a values of deprotonating DMPA yields the following equations for the fractions of DMPA molecules with one protonation f_{1H} and two protonations f_{2H}

$$f_{1H} = \frac{10^{pH_l - pK_{a1}}}{1 + 10^{pH_l - pK_{a1}} + 10^{2pH_l - pK_{a1} - pK_{a2}}}$$
$$f_{2H} = \frac{1}{1 + 10^{pH_l - pK_{a1}} + 10^{2pH_l - pK_{a1} - pK_{a2}}} \quad (2)$$

and the fraction of PA with no protons (0 state, charge 2−) is given by

$$f_0 = 1 - f_{1H} - f_{2H} = \frac{10^{2pH_l - pK_{a1} - pK_{a2}}}{1 + 10^{pH_l - pK_{a1}} + 10^{2pH_l - pK_{a1} - pK_{a2}}} \quad (3)$$

In this study, pK_{a1} and pK_{a2} were set as 3.0 and 7.1, respectively. Although the second pK_a is in the range between 7.0 and 7.9,[10] the actual differences from using values in this range are within experimental uncertainty. pH_l refers to the *local* pH value, which we computed using the Poisson−Boltzmann equation. Figure 4 shows that the predictions obtained using eq 2 (curve denoted by $K_1 = 0$ and $K_2 = 0$ in the figure) for the fraction of Ca^{2+} ions per molecule in DMPA and DHDP, respectively, are only slightly different at high pH $\gtrsim 7$ (approximately 0.5 Ca^{2+} per molecule), in clear disagreement with the experiment in a way that is not captured by eq 2. In this regard, recall that, for ions that bind weakly to the headgroup, as is the case for monovalent ions, eq 2 should still provide an accurate description. The effect shown in Figure 4 is dramatically enhanced by ion multivalency. Indeed, studies with monovalent Cs^+ did not show significant differences between DMPA and DHDP at physiological pH,[32] as predicted by eq 2.

We therefore include strong electrostatic binding of Ca^{2+} to PA considering the chemical reactions

$$PA^{2-} + Ca^{2+} \leftrightarrows (PA)Ca, \quad K_1$$
$$(PAH)^- + Ca^{2+} \leftrightarrows [(PA)HCa]^+, \quad K_2 \quad (4)$$

dx.doi.org/10.1021/jp303840a | J. Phys. Chem. B 2012, 116, 7213−7220

where K_1 and K_2 are the equilibrium (or binding) constants associated with these reactions. Describing long-range electrostatic forces with equilibrium constants is conceptually incorrect, but as extensively discussed,[51] binding constants can be justified from fundamental theories in many circumstances. Furthermore, the success of the approach to a wide range of studies in phospholipid bilayers[52] and monolayers[53] provides confidence in the validity of the proposed model.

The generalization of eq 2 that includes the two binding reactions in eqs 4 adds two additional interfacial species, namely, PA^{2-} with a bound Ca^{2+} ion, as well as the fraction of $(PAH)^{-}$ with a bound Ca^{2+} ion. In this way, the fractions for each species are found as (compare with eq 2)

$$f_{2H} = 1/(1 + 10^{pH_l - pK_{a1}} + 10^{2pH_l - pK_{a1} - pK_{a2}} + K_1[Ca^{2+}]10^{pH_l - pK_{a1}} + K_2[Ca^{2+}]10^{2pH_l - pK_{a1} - pK_{a2}})$$

$$f_{1H} = (10^{pH_l - pK_{a1}})/(1 + 10^{pH_l - pK_{a1}} + 10^{2pH_l - pK_{a1} - pK_{a2}} + K_1[Ca^{2+}]10^{pH_l - pK_{a1}} + K_2[Ca^{2+}]10^{2pH_l - pK_{a1} - pK_{a2}})$$

$$f_{Ca} = (K_1[Ca^{2+}]10^{pH_l - pK_{a1}})/(1 + 10^{pH_l - pK_{a1}} + 10^{2pH_l - pK_{a1} - pK_{a2}} + K_1[Ca^{2+}]10^{pH_l - pK_{a1}} + K_2[Ca^{2+}]10^{2pH_l - pK_{a1} - pK_{a2}})$$

$$f_{HCa} = (K_2[Ca^{2+}]10^{2pH_l - pK_{a1} - pK_{a2}})/(1 + 10^{pH_l - pK_{a1}} + 10^{2pH_l - pK_{a1} - pK_{a2}} + K_1[Ca^{2+}]10^{pH_l - pK_{a1}} + K_2[Ca^{2+}]10^{2pH_l - pK_{a1} - pK_{a2}}) \quad (5)$$

where f_{Ca} and f_{HCa} denote the fractions of PA molecules with one Ca^{2+} and one HCa^{+}, respectively, per molecule. In the absence of binding ($K_1 = K_2 = 0$), eq 5 reduces to eq 2. Physically, the *local* concentration of the binding species (Ca^{2+}, in this case), which we computed from the Poisson–Boltzmann equation, competes with the protons in binding to the lipid. Although the use of Poisson–Boltzmann theory is somewhat inappropriate for a highly charged surface and multivalent ionic solutions, this approximation is reasonable within the experimental error in this study.

The values of the constants can be estimated from relatively simple arguments (see Table 1 in ref 45, where $K_1 \approx 9$ and $K_2 \approx 631$) or more sophisticated calculations[51] yielding $K_1 \approx 10$ M^{-1} and $K_2 \approx 500$ M^{-1}. Physically, the large values of these equilibrium constants favor a situation in which binding of Ca^{2+} ions becomes favorable to protonation, thus enhancing the deprotonation of PA beyond what is predicted from the generalized Henderson–Hasselbalch formula (eq 2). Quantitative results for the fraction of Ca^{2+} ions per molecule, plotted in Figure 4, show an excellent agreement with experimental results. Recall that the values of K_1 and K_2 were estimated from theory and were not obtained from fitting. Yet, to assess the robustness of the theoretical model, different values of K_2 were tested, showing consistent results within the experimental errors. From the theoretical model in eq 5, more details on the structure of PA domains as a function of pH is provided. Plotted in Figure 5 are the fractions of different species of PA, thus showing that, at low pH (up to ~5), PA never becomes fully deprotonated, whereas at physiological pH (~7), the domain basically consists of doubly deprotonated PA molecules with a large majority of Ca^{2+} ions bound to it. Obviously, in the intermediate cases, more species have a significant presence.

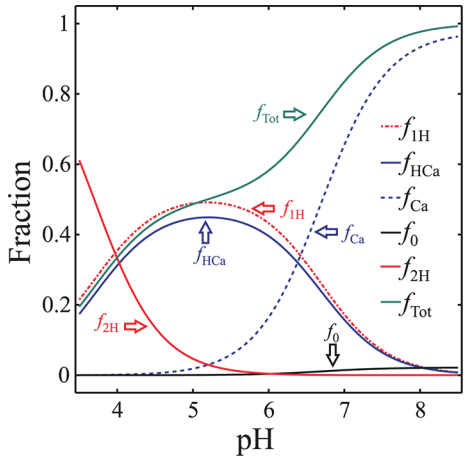

Figure 5. Relative fraction for each PA species, as defined in eq 5. The fraction of calcium ions per PA is shown as f_{Tot}. The $K_1 = 10$ and $K_2 = 500$ values were predicted from theory and agree with the experimental results.

CONCLUSIONS

Employing surface-sensitive X-ray scattering and spectroscopic techniques we determined the binding of Ca^{2+} per phospholipid molecule in monolayers of DMPA or DHDP. DHDP was investigated as a control experiment, because it is identical to PA except that it has two protonation states compared to the three of PA. At low pH (~3), the distributions of Ca^{2+} are nearly the same for the two molecules, but they differ very significantly as the pH is increased. This deprotonation observed in PA is explained by a theoretical model, demonstrating that the electrostatic correlations between Ca^{2+} (or, more generally, any multivalent ions) and phosphomonoester groups is directly responsible for enhanced deprotonation. The detailed analysis of XR and XF strongly suggests that solvated Ca^{2+} ions bind to phosphomonoester and diester groups with partial dehydration, in agreement with numerical simulations.[17]

The origin of the binding constants of Ca^{2+} ions to phosphate groups is entirely due to classical electrostatic forces, but binding constants due to other interactions such as hydrogen bonds can also be described by equilibrium constants. The approach used in eq 5 for Ca^{2+} ions can be generalized to lipids or proteins containing amine or hydroxyl groups using appropriate binding constants K_1 and K_2 that account for the effects of hydrogen bonding, as depicted schematically in Figure 6. In this way, it is shown that the so-called switch mechanism[11] is also described by this model, which thus becomes a general model for predicting the protonation state of PA in a

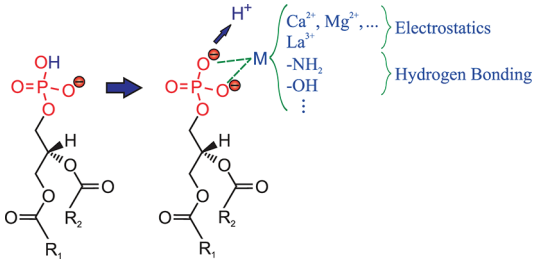

Figure 6. Schematic representation of induced deprotonation of PA in the presence of multivalent cations or amine or hydroxyl groups.

dx.doi.org/10.1021/jp303840a | J. Phys. Chem. B 2012, 116, 7213–7220

completely general scenario involving the influences of both ionic strength and hydrogen bonding (see Figure 6). We recall a recent model on the switch mechanism by Mengistu et al.[13] that has some overlap with the present model, where the role of the binding constant is played by an attractive potential.

The studies of Labbez et al.[21] have shown that, in silica interfaces, electrostatic correlations lead to enhanced deprotonation, in agreement with the results reported in this study. Yet, the fact that PA has two deprotonation states that are coupled (see eq 5) leads to a dramatic enhancement of the surface charge. Indeed, as reported by Labbez et al., effects accounting for electrostatic correlations and charge discreteness enhance deprotonation by 10% or 20% in silica for both monovalent and divalent ions, whereas for PA, the effect is more dramatic, as it leads to a small effect for monovalent ions (zero within the admittedly large experimental errors) but 100% for divalent ions.

Our results also have implications for phosphoinositides, as the charges of these molecules arise from the deprotonation of phosphomonoester groups. The most well-studied PIPs have two phosphomonoester groups (PIP_2), thus leading to a more complex situation than for PA. Recently, the pK_a values for PIP_2 were determined,[54] and titration studies for monovalent type were shown to be qualitatively consistent with the Henderson–Hasselbalch formula,[55] although a considerably less accurate expression than eq 2 was used. More recent studies of PIP_2 with Ca^{2+} have shown a more complex behavior.[56] The model and results covered in this work can be used to directly describe those results.

Recent in vivo studies[57,58] have provided strong evidence that PA acts as a pH biosensor, showing dramatic changes in protonation state as the intracellular pH varies, for example, by glucose starvation, with dramatic consequences in different signaling pathways. Clearly, a thorough investigation of the protonation state in real cells is beyond the scope of this work, but based on the results presented, we speculate that the presence of divalent ions (such as Mg^{2+}, typically present in the millimolar range) or other multivalent ions is crucial in the regulation of the protonation observed in PA. In addition to the general interest in physical chemistry, the characterization of the protonation state of PA has consequences for understanding how cellular membranes perform their function.

■ ASSOCIATED CONTENT

Supporting Information

Surface pressure versus molecular area isotherms and detailed analysis of X-ray reflectivity data and X-ray fluorescence data. This material is available free of charge via the Internet at http://pubs.acs.org.

■ AUTHOR INFORMATION

Corresponding Author

*E-mail: vaknin@ameslab.gov.

Notes

The authors declare no competing financial interest.

■ ACKNOWLEDGMENTS

The work of W.W., N.A.A., and D.V. at Ames Laboratory was supported by the Office of Basic Energy Sciences, U.S. Department of Energy, under Contract DE-AC02-07CH11358. The work of A.T. was supported by the NSF through Grant CAREER DMR-0748475.

■ REFERENCES

(1) Hannun, Y. A. *J. Biol. Chem.* **1994**, *269*, 3125–3128.
(2) Wang, X.; Devaiah, S. P.; Zhang, W.; Welti, R. *Prog. Lipid Res.* **2006**, *45*, 250–278.
(3) McLaughlin, S.; Wang, J.; Gambhir, A.; Murray, D. *Annu. Rev. Biophys. Biomol. Struct.* **2002**, *31*, 151–175.
(4) Di Paolo, G.; De Camilli, P. *Nature* **2006**, *443*, 651–657.
(5) Ile, K. E.; Schaaf, G.; Bankaitis, V. A. *Nat. Chem. Biol.* **2006**, *2*, 576–583.
(6) Yeung, T.; Gilbert, G. E.; Shi, J.; Silvius, J.; Kapus, A.; Grinstein, S. *Science* **2008**, *319*, 210–213.
(7) McLaughlin, S.; Murray, D. *Nature* **2005**, *438*, 605–611.
(8) Bu, W.; Vaknin, D.; Travesset, A. *Phys. Rev. E* **2005**, *72*, 060501–060504.
(9) Bu, W.; Vaknin, D.; Travesset, A. *Langmuir* **2006**, *22*, 5673–5681.
(10) Kooijman, E. E.; Carter, K. M.; van Laar, E. G.; Chupin, V.; Burger, K. N. J.; de Kruijff, B. *Biochemistry* **2005**, *44*, 17007–17015.
(11) Kooijman, E. E.; Tieleman, D. P.; Testerink, C.; Munnik, T.; Rijkers, D. T. S.; Burger, K. N. J.; de Kruijff, B. *J. Biol. Chem.* **2007**, *282*, 11356–11364.
(12) Kooijman, E. E.; Burger, K. N. J. *Biochim. Biophys. Acta* **2009**, *1791*, 881–888.
(13) Mengistu, D. H.; Kooijman, E. E.; May, S. *Biochim. Biophys. Acta* **2011**, *1808*, 1985–1992.
(14) Vaknin, D.; Krüger, P.; Lösche, M. *Phys. Rev. Lett.* **2003**, *90*, 178102–178105.
(15) Bu, W.; Flores, K.; Pleasants, J.; Vaknin, D. *Langmuir* **2009**, *25*, 1068–1073.
(16) Pittler, J.; Bu, W.; Vaknin, D.; Travesset, A.; McGillivray, D. J.; Lösche, M. *Phys. Rev. Lett.* **2006**, *97*, 046102–046105.
(17) Faraudo, J.; Travesset, A. *Biophys. J.* **2007**, *92*, 2806–2818.
(18) Berridge, M. J.; Bootman, M. D.; Lipp, P. *Nature* **1998**, *395*, 645–648.
(19) Karlsson, M.; Craven, C.; Dove, P. M.; Casey, M. *Aquat. Geochem.* **2001**, *7*, 13–32.
(20) Lorenz, C. D.; Crozier, P. S.; Anderson, J. A.; Travesset, A. *J. Phys. Chem. C* **2008**, *112*, 10222–10232.
(21) Labbez, C.; Jönsson, B.; Skarba, M.; Borkovec, M. *Langmuir* **2009**, *25*, 7209–7213.
(22) Hauser, H.; Shipley, G. G. *Biochemistry* **1984**, *23*, 34–41.
(23) Huster, D.; Arnold, K.; Gawrisch, K. *Biophys. J.* **2000**, *78*, 3011–3018.
(24) Casal, H. L.; Mantsch, H. H.; Hauser, H. *Biochemistry* **1987**, *26*, 4408–4416.
(25) Mattai, J.; Hauser, H.; Demel, R. A.; Shipley, G. G. *Biochemistry* **1989**, *28*, 2322–2330.
(26) Laroche, G.; Dufourc, E. J.; Dufourcq, J.; Pézolet, M. *Biochemistry* **1991**, *30*, 3105–3114.
(27) Altenbach, C.; Seelig, J. *Biochemistry* **1984**, *23*, 3913–3920.
(28) Takahashi, H.; Murase, Y.; Kurihara, K.; Hatta, I.; Arakawa, E.; Takeshita, K.; Matsushita, T. *Jpn. J. Appl. Phys.* **1996**, *35*, 1092–1095.
(29) Kewalramani, S.; Hlaing, H.; Ocko, B. M.; Kuzmenko, I.; Fukuto, M. *J. Phys. Chem. Lett.* **2010**, *1*, 489–495.
(30) Schalke, M.; Lösche, M. *Adv. Colloid Interface Sci.* **2000**, *88*, 243–274.
(31) Kooijman, E. E.; Vaknin, D.; Bu, W.; Joshi, L.; Kang, S. W.; Gericke, A.; Mann, E. K.; Kumar, S. *Biophys. J.* **2009**, *96*, 2204–2215.
(32) Bu, W.; Vaknin, D. *J. Appl. Phys.* **2009**, *105*, 084911–084916.
(33) Yun, W.; Bloch, J. M. *J. Appl. Phys.* **1990**, *68*, 1421–1428.
(34) Daillant, J.; Bosio, L.; Benattar, J. J.; Blot, C. *Langmuir* **1991**, *7*, 611–614.
(35) Supporting Information.
(36) Parratt, L. G. *Phys. Rev.* **1954**, *95*, 359–369.
(37) Gibaud, A. In *X-Ray and Neutron Reflectivity: Principles and Applications*; Daillant, J., Gibaud, A., Eds.; Lecture Notes in Physics Monographs; Springer-Verlag: Berlin, 1999; Vol. *58*, Chapter 3.

(38) Tolan, M. *X-Ray Scattering from Soft-Matter Thin Films: Materials Science and Basic Research*; Springer Tracts in Modern Physics; Springer-Verlag: Berlin, 1999; Vol. *148*, Chapter 2.
(39) Als-Nielsen, J.; McMorrow, D. *Elements of Modern X-ray Physics*, 2nd ed.; John Wiley & Sons: London, 2011; Chapter 3.
(40) Vaknin, D. In *Characterization of Materials*; Kaufmann, E. N., Ed.; John Wiley & Sons: New York, 2003; pp 1027−1047.
(41) Wang, W.; Park, R. Y.; Meyer, D. H.; Travesset, A.; Vaknin, D. *Langmuir* **2011**, *27*, 11917−11924.
(42) Wang, W.; Park, R. Y.; Travesset, A.; Vaknin, D. *Phys. Rev. Lett.* **2011**, *106*, 056102−056105.
(43) Wang, W.; Bu, W.; Wang, L.; Palo, P. E.; Mallapragada, S.; Nilsen-Hamilton, M.; Vaknin, D. *Langmuir* **2012**, *28*, 4274−4282.
(44) Kjaer, J. *Phys. B (Amsterdam, Neth.)* **1994**, *198*, 100−109.
(45) Travesset, A.; Vaknin, D. *Europhys. Lett.* **2006**, *74*, 181−187.
(46) Vaknin, D.; Kjaer, K.; Als-Nielsen, J.; Lösche, M. *Biophys. J.* **1991**, *59*, 1325−1332.
(47) Ohtaki, H.; Radnai, T. *Chem. Rev.* **1993**, *93*, 1157−1204.
(48) Jalilehvand, F.; Spångberg, D; Lindqvist-Reis, P.; Hermansson, K.; Persson, I.; Sandström, M. *J. Am. Chem. Soc.* **2001**, *123*, 431−441.
(49) Bakó, I.; Hutter, J.; Pálinkás, G. *J. Chem. Phys.* **2002**, *117*, 9838−9843.
(50) Jeremic, A.; Cho, W. J.; Jena, B. P. *J. Biol. Phys. Chem.* **2004**, *4*, 139−142.
(51) Travesset, A.; Vangaveti, S. *J. Chem. Phys.* **2009**, *131*, 185102−185112.
(52) McLaughlin, S. *Annu. Rev. Biophys. Biophys. Chem.* **1989**, *18*, 113−136.
(53) Bloch, J. M.; Yun, W. *Phys. Rev. A* **1990**, *41*, 844−862.
(54) Kooijman, E. E.; King, K. E.; Gangoda, M.; Gericke, A. *Biochemistry* **2009**, *48*, 9360−9371.
(55) Levental, I.; Janmey, P. A.; Cēbers, A. *Biophys. J.* **2008**, *95*, 1199−1205.
(56) Ellenbroek, W. G.; Wang, Y.; Christian, D. A.; Discher, D. E.; Janmey, P. A.; Liu, A. J. *Biophys. J.* **2011**, *101*, 2178−2184.
(57) Young, B. P.; Shin, J. J. H.; Orij, R.; Chao, J. T.; Li, S. C.; Guan, X. L.; Khong, A.; Jan, E; Wenk, M. R.; Prinz, W. A.; Smits, G. J.; Loewen, C. J. R. *Science* **2010**, *329*, 1085−1088.
(58) Shin, J. J. H.; Loewen, C. J. R. *BMC Biol.* **2011**, *9*, 85−94.